Encoding and decoding messages with chaotic lasers

P. M. Alsing*
High Performance Computing Center, University of New Mexico, 1601 Central NE, Albuquerque, New Mexico 87131

A. Gavrielides† and V. Kovanis‡
Nonlinear Optics Center, Phillips Laboratory, 3550 Aberdeen Avenue SE, Kirtland Air Force Base, New Mexico 87117-5776

R. Roy and K. S. Thornburg, Jr.
School of Physics, Georgia Institute of Technology, Atlanta, Georgia 30332-0430
(Received 5 August 1996)

We investigate the structure of the strange attractor of a chaotic loss-modulated solid-state laser utilizing return maps based on a combination of intensity maxima and interspike intervals, as opposed to those utilizing Poincaré sections defined by the intensity maxima of the laser ($\dot{I}=0,\ddot{I}<0$) alone. We find both experimentally and numerically that a simple, intrinsic relationship exists between an intensity maximum and the pair of preceding and succeeding interspike intervals. In addition, we numerically investigate encoding messages on the output of a chaotic transmitter laser and its subsequent decoding by a similar receiver laser. By exploiting the relationship between the intensity maxima and the interspike intervals, we demonstrate that the method utilized to encode the message is vital to the system's ability to hide the signal from unwanted deciphering. In this work alternative methods are studied in order to encode messages by modulating the magnitude of pumping of the transmitter laser and also by driving its loss modulation with more than one frequency. [S1063-651X(97)01808-4]

PACS number(s): 05.40+j, 42.50.Lc

I. INTRODUCTION

There has been great interest in the use of chaotic signals as the carriers of analog and digital information over the last few years, initiated by the work of Pecora and Carroll [1], who suggested that synchronized chaotic systems could be employed to encode and decode messages in real time. Recent experiments have demonstrated that using chaos to communicate is practically feasible with electronic circuits [2,3]. The typical frequencies of the chaotic carrier wave forms in these circuits is of the order of 10 kHz, and even with the prospects of speeding up these circuits by several orders of magnitude, it is still of interest to consider communication with chaotic optical signals which have the potential for even higher information transmission and reception rates.

Two groups have experimentally demonstrated that chaotic lasers can be synchronized. Roy and Thornburg [4] showed that synchronization could be achieved in a pair of pump-modulated Nd:YAG (yttrium aluminum garnet) lasers by altering the mutual evanescent coupling between the lasers. Sugawara *et al.* [5] demonstrated synchronization of two CO_2 lasers by injecting the output of a master laser into a receiver laser with a saturable absorber. Colet and Roy [6] have suggested a scheme involving the synchronization of a chaotic Nd:YAG carrier laser to a receiving laser, and the subsequent decoding of the hidden message in real time by subtraction of the receiver input from its output. The sharp pulses generated by loss modulation of the laser serve as a natural background for encoding and camouflaging digital information. The authors demonstrated the validity of their proposed scheme in numerical simulations. This idea has been extended to a model of synchronized chaotic semiconductor lasers by Mirasso *et al.*, who have included the effects of a fiber optic channel on the information processing [7].

In this paper we explore issues related to the communication scheme as proposed in [6]. In Sec. II the loss-modulated Nd:YAG laser model is introduced along with techniques for encoding and decoding of messages. Next, in Sec. III we present an analysis of numerical and experimental time series via return maps based upon interspike intervals. We find that a simple relationship exists between an intensity peak and interspike intervals that precede and follow the peak. The consequences of this relationship on the issue of deciphering the message encrypted in the chaotic carrier is explored in Sec. IV. Two schemes for encoding information are then introduced that make it more difficult to decipher the message. These consist of laser parameter modulation of the transmitter to encode the message and the use of quasiperiodic parameter modulation in both transmitter and receiver, so that the interspike interval return maps become ineffectual as deciphering tools, while the receiver's ability to decode the message is retained. The main results of the paper are summarized in Sec. V, and conclusions are drawn.

II. SCHEME FOR COMMUNICATING WITH SYNCHRONIZED CHAOTIC LASERS

The scheme proposed by Colet and Roy [6] for communicating signals via chaotic synchronized lasers is composed of a pair of loss-modulated Nd:YAG lasers operated in the chaotic regime. The hidden signal is decoded by subtraction

*Electronic address: alsing@arc.unm.edu
†Electronic address: tom@photon.plk.af.mil
‡Electronic address: kovanis@xaos.plk.af.mil

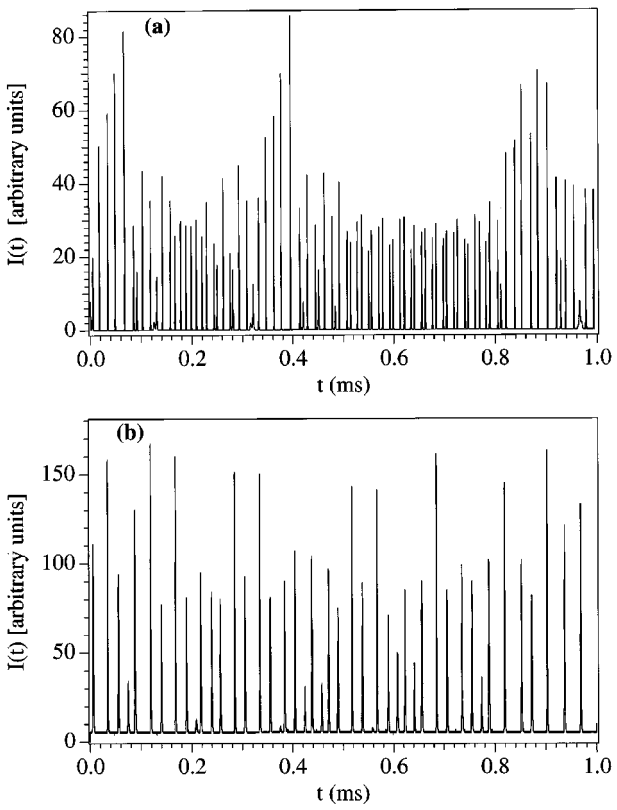

FIG. 1. (a) Numerical simulation of the loss-modulated Nd:YAG chaotic laser, Eqs. (2.1), $\alpha_{0T}=\alpha_{0R}=0.01$, $\alpha_1=2.0\times10^{-4}$, $\Omega=541.6$ ms^{-1}, $P_T=P_R=0.03$, $\epsilon_T=\epsilon_R=8.33\times10^{-9}$ s^{-1}, $\omega_R-\omega_T=50\,000$ rad/s, and $\kappa=10^{-4}$; (b) experimental data from a loss-modulated Nd:YAG chaotic laser operated one-third above threshold with parameters as in (a) except for $\tau_c=1/\gamma_c=0.45$ ns.

of the receiver and transmitter intensities.

The model for the transmitting laser is described by [6,9]

$$\frac{dE_T}{dt}=\gamma_c(G_T-\alpha_{0T}-\alpha_1\cos\Omega t)E_T+i\omega_T E_T+\sqrt{\epsilon_T}\eta_T, \tag{2.1a}$$

$$\frac{dG_T}{dt}=\gamma_f[P_T-G_T(1+|E_T|^2)], \tag{2.1b}$$

where E_T is the complex, slowly varying amplitude of the electric field, G_T is the gain of the active medium, $\tau_c=1/\gamma_c=$ 450 ps is the cavity round-trip time, $\tau_f=1/\gamma_f=240$ μs is the decay time of the upper lasing level, ω_T is the detuning of the laser frequency from the nearest empty cavity mode, P_T is the pump parameter, ϵ_T is the spontaneous emission noise strength, and η_T is a complex Gaussian white noise term of zero mean and correlation $\langle\eta_T(t)\eta_T^*(t')\rangle=2\delta(t-t')$. The loss modulation is given by $\alpha_T(t)\equiv\alpha_{0T}+\alpha_1\cos(\Omega t)$ where $\alpha_1/\alpha_{0T}\ll1$. The modulation frequency Ω is chosen to be close to a submultiple of the relaxation frequency $\omega_r=\sqrt{2\gamma_c\gamma_f(P_T-\alpha_{0T})}$.

The output intensity of the chaotic laser is a series of irregularly spaced pulses having a spiky appearance, as evidenced in the numerical simulation of a loss-modulated solid-state laser in Fig. 1(a) and in similar experimental data such as Fig. 1(b), which are recorded at slightly different parameter values. Although the numerical simulation and the experimental data appear similar with respect to the irregularity of the intensity maxima, the temporal sequence of intensity maxima appears more regularly spaced in the experimental data than in the numerical simulation. We will return to this point, and to a more detailed description of the output intensity, in Sec. III.

The equations describing the receiving laser in which the encoded signal from the transmitter laser has been injected are given by

$$\frac{dE_R}{dt}=\gamma_c(G_R-\alpha_{0T}-\alpha_1\cos\Omega t)E_R+i\omega_R E_R+\sqrt{\epsilon_R}\eta_R-\kappa A_b\gamma_c\left(E_R-\frac{A_S}{A_b}E_T\right), \tag{2.2a}$$

$$\frac{dG_R}{dt}=\gamma_f[P_R-G_R(1+|E_R|^2)]. \tag{2.2b}$$

In the above equations all variables have the same meaning as for the transmitter. In addition, the modulated loss coefficient of the receiver, $\alpha_R(t)\equiv\alpha_{0R}+\alpha_1\cos(\Omega t)$ is operated at the condition for synchronization (i.e., $E_R=E_T$), $\alpha_{0R}=\alpha_{0T}+\kappa$. The quantity $\kappa\ll\alpha_{0T}$ is the coupling coefficient between the transmitting and receiving laser which also accounts for any losses in the transmission process [9].

The transmission coefficients A in Eqs. (2.2) describe the encoding of the signal on the external output of the transmitting laser. The output intensity of the transmitting laser is slightly attenuated by an external filter by a fixed bias factor A_b, so that the intensity at the receiver is given by $E_T'=\kappa A_b E_T$. This implies that synchronization is achieved when no signal is encoded at a setting of $\alpha_{0R}=\alpha_{0T}+\kappa A_b$. To encode a ''1'' bit, the transmission is increased a few percent to $A_S>A_b$, while to send a ''-1'' bit the transmission is decreased a few percent to $A_S<A_b$. Thus the message is encoded as small amplitude modulations of the spiky, high intensity output of the transmitting laser. To avoid encoding signals on the low intensity pulses, the pulses are monitored before attenuation and only those pulses whose intensity exceeds some predetermined, fixed threshold intensity are used for encoding.

In Eq. (2.2a) the signal difference term can be written as

$$-\kappa A_b\gamma_c\left(E_R-\frac{A_S}{A_b}E_T\right)=-\kappa A_b\gamma_c(E_R-E_T)+\kappa\gamma_c(A_S-A_b)E_T. \tag{2.3}$$

The first term $-\kappa A_b\gamma_c(E_R-E_T)$ is responsible for the synchronization of the transmitter laser to the receiver laser. For values of κ above some threshold, the damping is sufficient to drive the signal difference to zero, thereby synchronizing the receiver to the chaotic transmitter carrier wave. If $\kappa\gamma_c(A_S-A_b)E_T$ is small, the transmitter carrier wave plus signal is then entrained by the receiver laser. The signal can be deciphered precisely because it is a small perturbation of the carrier signal. As long as the κ is above some threshold value (which usually needs to be found empirically, see Fig.

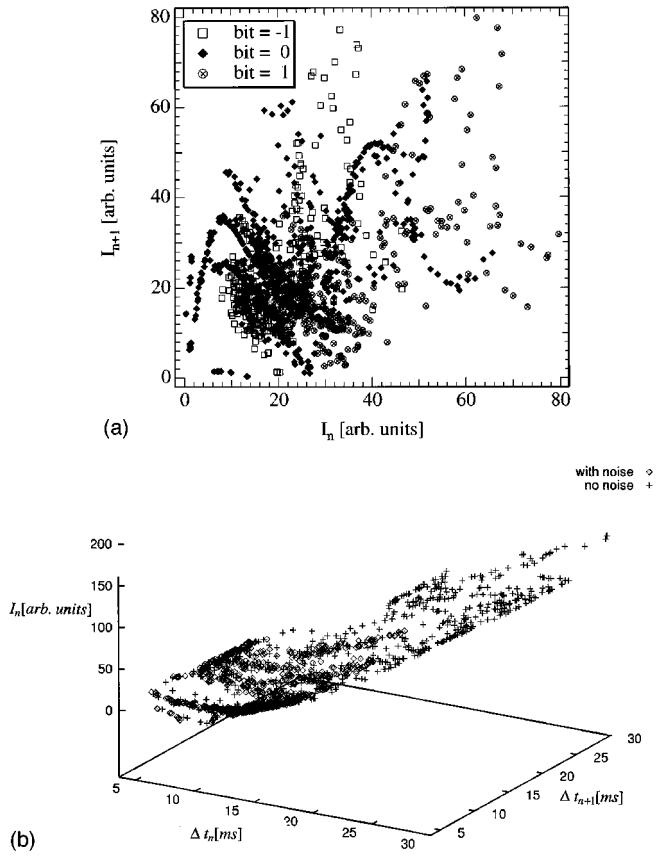

FIG. 2. (a) Plot of intensity maxima return map $I_T(n+1)$ vs $I_T(n)$ with data from Fig. 1(a); (b) same data plotted as intensity maxima $I_T(n)$ vs the interspike intervals $\Delta t_T(n+1)=t_T(n+1)-t_T(n)$ and $\Delta t_T(n)=t_T(n)-t_T(n-1)$.

2 in [6]) and the signal amplitude is small relative to the carrier wave, the carrier wave plus the encoded signal remains entrained by the output of the receiving laser.

The encoded signal can then be extracted as the integrated intensity difference M [6],

$$M=\int_{\text{pulse}}(|A_S E_T|^2-|A_b E_R|^2)dt. \tag{2.4}$$

The quantity M will equal zero when no signal is sent, $A_S=A_b$, and will have a strong positive (negative) value when a ''1'' (''−1'') bit, $A_S>A_b$ ($A_S<A_b$), is being sent. Figure 2(a) shows a first return map of the numerically generated receiver intensity $I_R(n+1)$ vs $I_R(n)$, evaluated at the intensity maxima, when a signal has been encoded on the transmitter. The carrier wave maxima, and the ''1'' and ''−1'' bit are depicted by the diamonds, pluses, and squares, respectively. One sees that the encoded signal is seemingly inextricably mixed with the carrier wave. Higher dimensional intensity peak return maps, $I(n+1)$ versus $\{I(n),I(n-1),I(n-2),\ldots\}$, offer no additional help towards unraveling the signal from the carrier [8].

III. ANALYSIS VIA INTERSPIKE INTERVALS

A useful representation of the data occurs when one considers return maps based not solely on intensity maxima, but rather on a combination of the intensity maxima with the time intervals between intensity maxima, which we call the *interspike intervals* (ISI). In a recent paper, Sauer [10] proposed the use of interspike intervals as a means for attractor reconstruction from time series, in analogy with Takens' theorem [11]. In this work we use the interspike intervals to find a useful relationship between the ISI and the intensity maxima of a chaotic loss-modulated solid-state laser.

Figure 2(b) is a plot of numerically generated transmitter laser intensity maxima $I_T(n)$ of Fig. 1(a) occuring at time $t(n)$ versus the pair of interspike intervals $\Delta t_T(n+1)$ and $\Delta t_T(n)$, where $\Delta t_T(n+1)\equiv t_T(n+1)-t_T(n)$. Here $\Delta t_T(n+1)$ is the time between the nth intensity maxima $I_T(n)$ at time $t_T(n)$ and the occurrence of the next intensity maxima at time $t_T(n+1)$. Similarly, $\Delta t_T(n)$ is the time between the nth intensity maxima $I_T(n)$ at time $t_T(n)$ and the previous intensity maxima at time $t_T(n-1)$. A reconstruction of the attractor solely using interspike intervals, i.e., $\Delta t_T(n+1)$ versus $\Delta t_T(n)$ and $\Delta t_T(n-1)$ reveals no added information over a reconstruction solely using intensity maxima, $I(n+1)$ versus $I(n)$ and $I(n-1)$. It is the combination of intensity maxima and interspike intervals as shown in Fig. 2(b) which uncovers structure, and a relationship between physical quantities.

Figure 2(b) shows results of the numerical simulation with noise (''+'') and without the inclusion of noise (diamonds). The level of noise was chosen to be typical of that experienced in laboratory experiments (see Fig. 1 in [6]). Both the noise-free and noisy maxima fall on a nearly two-dimensional surface that is essentially planar. Figure 3(a) shows the intensity maxima of the noise-free simulation, while Fig. 3(b) shows the same plot from an edge-on view, that is $I_T(n)$ versus

$$\begin{aligned}&\cos(\theta)\Delta t_T(n+1)+\sin(\theta)\Delta t_T(n)\\&\quad=[\Delta t_T(n+1)+\Delta t_T(n)]/\sqrt{2}\\&\quad=[t_T(n+1)-t_T(n-1)]/\sqrt{2}.\end{aligned}$$

where the angle $\theta=\pi/4$ gave the optimal view. Here we clearly see an almost one dimensional structure of the return map. Figure 3(c) shows the noisy simulation with the similar, nearly one-dimensional structure in the return map, viewed edge on in Fig. 3(d). Note that the intensity maxima of the noisy simulation Fig. 3(c), fall on the same nearly two-dimensional surface of Fig. 3(a), but in that portion of the surface corresponding to lower intensity maxima. We return to this point shortly.

Figure 3(e) is an edge-on plot of the experimental data (diamonds) of Fig. 1(b). Because the experimental data was taken at parameter values slightly different from that of the numerical simulation, the temporal variation of the interspike intervals in Fig. 1(b) is on a finer scale. In fact, the data in Fig. 3(e) corresponds to the upper right-hand, high intensity maxima corner of the data of the numerical simulation, Fig. 3(c). However, even for this more uniform variation of the interspike intervals, a plot of the intensity maxima-ISI return map reveals structure and a relationship between physical variables. The experimental data is again essentially planar as evidenced by a global least squares fit of the experimental intensity maxima to the experimentally derived interspike

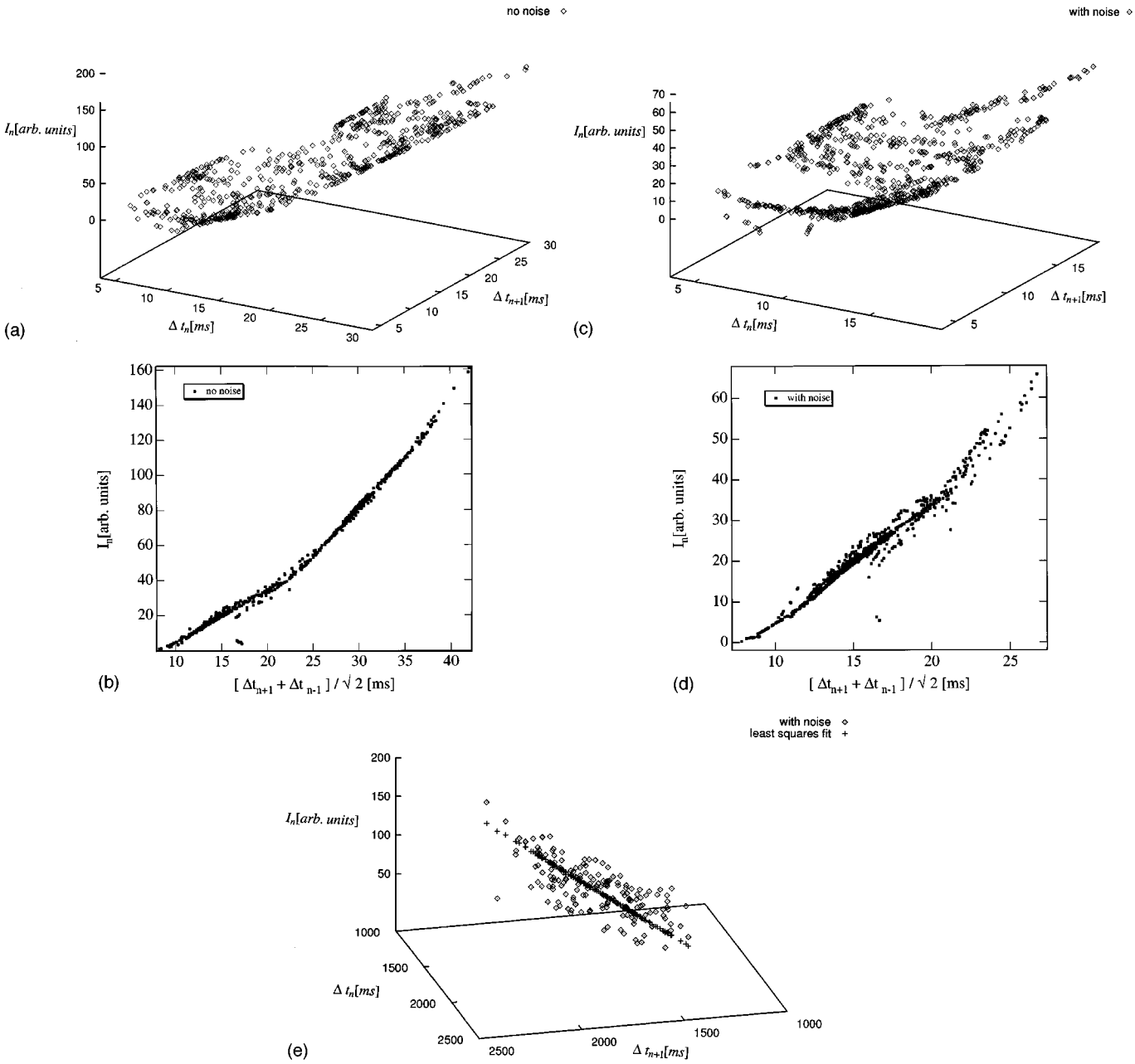

FIG. 3. Intensity-interspike intervals return maps of the transmitter laser: (a) $I_T(n)$ vs $\Delta t_T(n+1)=t_T(n+1)-t_T(n)$ and $\Delta t_T(n)=t_T(n)-t_T(n-1)$ corresponding to Fig. 1(a); (b) edge-on view of (a); (c) part (a), with noise, $\epsilon_T=\epsilon_R=8.33\times10^{-9}$ s^{-1}; (d) edge-on view of part (c); (e) edge-on view of experimental data (diamonds), Fig. 1(b), with global least square fit (''+'') of intensity maxima $I_T(n)$ to $\Delta t_T(n+1)$ and $\Delta t_T(n)$. Note that these data correspond to the upper right-hand corner (15–20 μs) of (c).

intervals $\Delta t_T(n+1)$ and $\Delta t_T(n)$. The plane of this least square fit of intensity maxima to ISI is shown in an edge-on view as the overlaid heavy straight line (''+'') in the center of Fig. 3(e). One should note that it is not important in plotting these return maps to utilize the precise maxima of the intensity, which may be hard to resolve in an actual experiment. Any convenient threshold value on the intensity spike could be used to replace $I_T(n)$, and $\Delta t_T(n)$ would then be measured as the time between successive crossings of this threshold.

If one were to plot a three-dimensional return map of the interspike intervals alone, i.e., $\Delta t_T(n+1)$ vs $\Delta t_T(n)$ and $\Delta t_T(n-1)$, the result would be an unfolding of the attractor, topologically equivalent to an unfolding utilizing only the intensity maxima, $I(n+1)$ vs $I(n)$ and $I(n-1)$. The significance of the nearly planar (linear) structure of the intensity-ISI return maps in Fig. 3(a) [Figs. 3(b) and 3(e)] is that it implies that there exists a nearly linear relationship between the intensity maxima $I_T(n)$ and the interspike intervals $\Delta t_T(n+1)$ and $\Delta t_T(n)$.

Schwartz and Erneux [12] explored this loss-modulated laser system and found explicit representations for the Poincaré mapping between the (dimensionless) gain and the ISI applicable to the period 1 and 2 orbits. Though it is not the goal of this paper, Figs. 3 suggest that such a map might be found also in the chaotic regime. They analyzed the periodi-

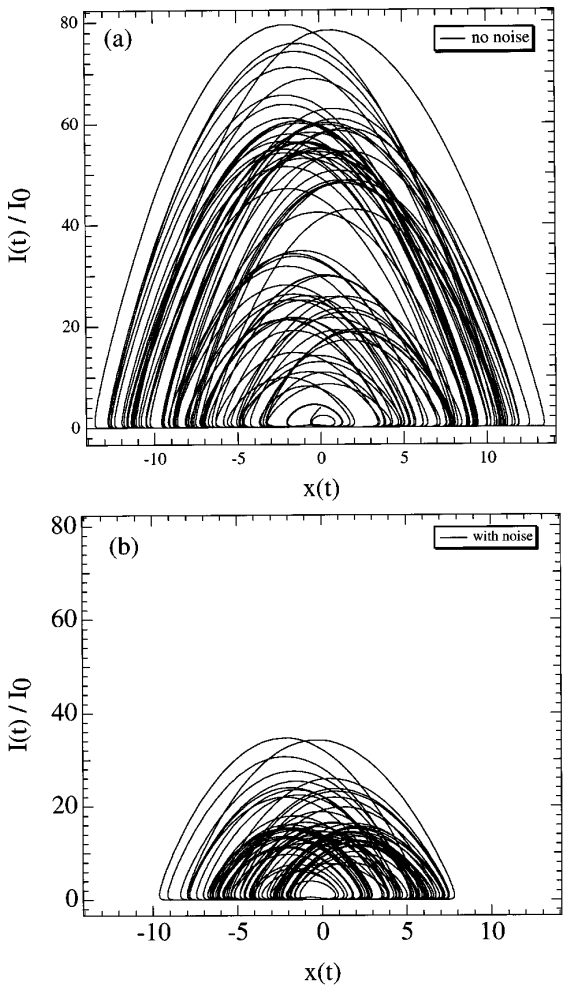

FIG. 4. Plot of scaled transmitter intensity $y(t)=[I_T(t)-I_{ss}]/I_{ss}$ vs the normalized gain $x(t)$ from Eq. (2.1): (a) no noise, (b) with noise. [I_{ss} is the steady-state intensity of the conservative system, which to lowest order approximates the system of equations in Eq. (2.1)]. The large intensity maxima occur when the previous intensity minima reach very low values.

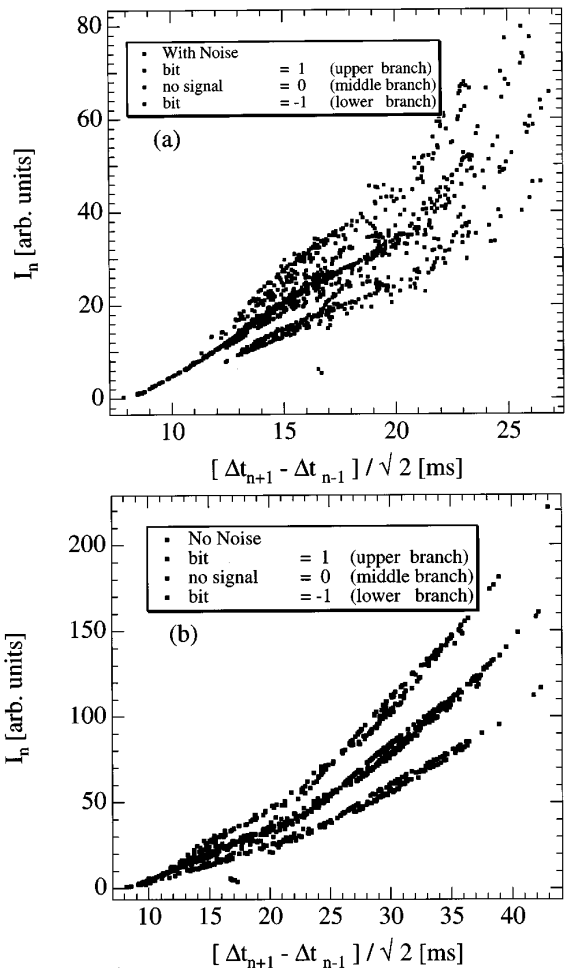

FIG. 5. Decoding of the signal hidden in the chaotic carrier of the transmitter laser by the return map of $I_T(n)$ vs $[t_T(n+1)-t_T(n-1)]/\sqrt{2}$. The transmitter laser has been modulated with $A_S=1.0\pm0.15A_b$, with $A_b=0.85$: Upper branch → ''1'' bit, middle branch → no signal, lower branch → ''−1'' bit. (a) no noise, (b) with noise.

cally driven laser system as a conservative system (to lowest order of approximation) plus small nonlinear terms. When dissipation is neglected, periodic orbits in the plane of the (dimensionless) gain x and intensity relative to the steady-state value of the conservative system $y=(I-I_{ss})/I_{ss}$, are rounded triangular closed orbits with a flat base parallel to the x axis at a value of $y\sim-1$ corresponding to zero intensity (see Fig. 4 and Fig. 5 in [12]). High intensity maxima correspond to the previous intensity minima reaching very low values, Fig. 4(a) where we plot the dimensionless intensity and gain $I_T(t)$ vs $G_T(t)$ from Eq. (2.1) as $y(t)$ vs $x(t)$. In the chaotic regime, the lowest order approximation of the laser system is still a conservative system, and this relationship between the height of the intensity maxima and period (and therefore ISI) is retained. With the inclusion of noise, Fig. 4(b), a minimum base line intensity is maintained, which correspondingly limits the maximum height of the intensity peaks. We see this in Fig. 3(a) where the noisy intensity maxima are restricted to the portion of the two-dimensional surface corresponding to smaller intensity peak heights and therefore, small values of the ISI.

IV. CONSEQUENCES FOR CHAOTIC COMMUNICATION

The regular structure of the intensity versus ISI return maps has important implications for communicating signals via a chaotic transmitter laser. As proposed by Colet and Roy [6], the transmitter laser encodes the signal by an amplitude modulation external to the laser. Since the transmitter is not intrinsically perturbed, Figs. 3 suggests that the intensity maxima-ISI return maps applied to the transmitter signal alone could be used to decode the signal. Figure 5(a) is a plot of the simulated transmitter intensity output maxima $I_T(n)$ vs the ISI combination $[t_T(n+1)-t_T(n-1)]/\sqrt{2}$, when the laser has been modulated with $A_S=1.0\pm0.15A_b$ with $A_b=0.85$, without the inclusion of noise. Signals were encoded only on intensity maxima with values approximately greater than 10. The middle branch is the no-signal maxima $A_S=A_b$, while the upper branch corresponds to a ''1'' bit $A_S=1.15A_b$, and the lower branch corresponds to a ''−1'' bit $A_S=0.85A_b$. Figure 5(b) is the corresponding simulation when noise has been included using a value of $\epsilon_T=\epsilon_R=8.33\times10^{-9}$ s^{-1}, typical of actual experiments [6,9]. Even though the noise smears the branches out some-

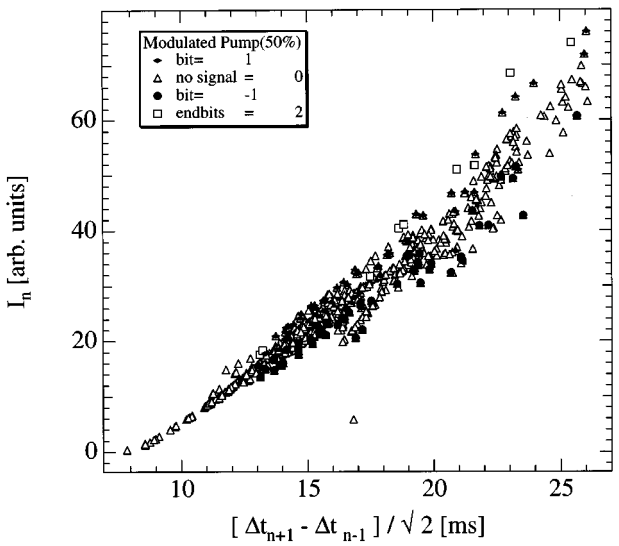

FIG. 6. The return map of the transmitter laser, $I_T(n)$ vs $[t_T(n+1)-t_T(n-1)]/\sqrt{2}$, when the transmitter laser pump has been modulated with $P_S=1.0\pm0.50P_T$ (no noise). Compared with Fig. 5(a), the signal branches corresponding to the encoded bits $\{1,-1\}$ have been merged with the no-signal branch.

what, they are still clearly distinguishable. Plots at 5% encoding modulation for $A_b=0.9$ show similar behavior of clearly distinguishable signal branches.

The signals embedded in the chaotic output of the transmitting laser were decipherable because of the inherent relationship between intensity maxima and interspike intervals exhibited in the intensity-ISI return maps. This encoding scheme, in which the transmitter laser intensity was modulated outside of the laser cavity, did not dynamically alter the relationship between intensity maxima and interspike intervals. Therefore, to encode and hide signals on the chaotic transmitter carrier we suggest that it would be more advantageous to have the encoding method fundamentally perturb the ISI. This can be achieved by modulating the transmitter pump across an intensity peak. The actual beginning and ending of the modulation could occur in the intensity troughs, as long as the pump change persists over the intensity peak. In Figure 6 we have simulated the intensity output of the transmitting laser when its pump has been modulated with $P_S=1.0\pm0.50P_T(t)$ and without the inclusion of noise. The resulting edge-on view of intensity-ISI return map for the transmitter shows that the attractor surfaces have been essentially merged together onto the no signal surface. Even if we were to look at the logarithmic signal differences, our success rate of distinguishing a ''±1'' bit from no-signal via the transmitter return maps is greatly diminished due to the severe overlapping of the surfaces. For smaller modulations or with the inclusion of noise, things only become more difficult. However, the signal *can* be decoded when the transmitting laser output is synchronized to the receiver and the integrated signal difference of Eq. (2.4) is utilized.

We point out an interesting feature of this encoding scheme that differs from the original encoding scheme in which the laser intensity is externally modulated. Figure 7(a) shows the decoded message bits (solid line) when the external intensity is used to encode the signal. The dashed line in this figure is the value of the discrete bits ''±1,'' encoded on

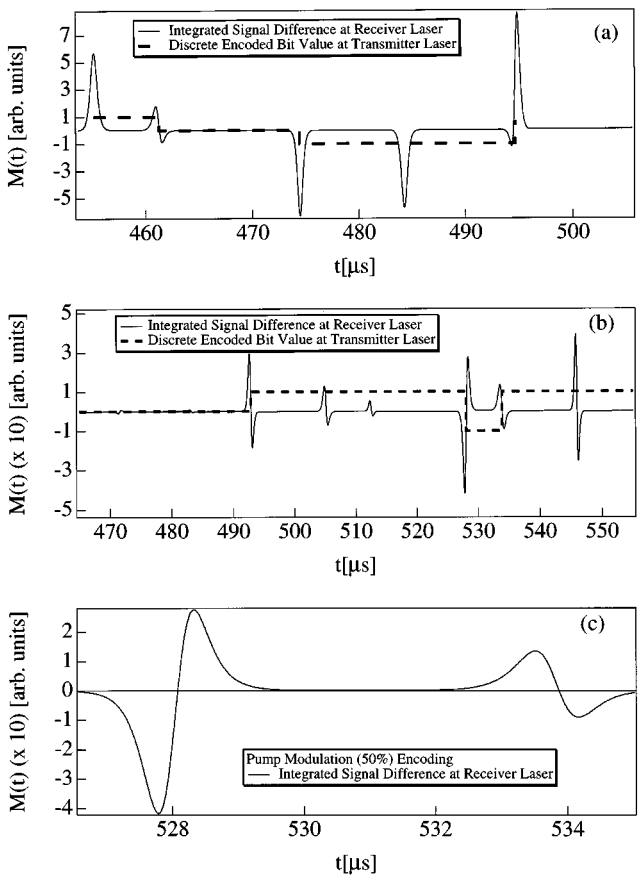

FIG. 7. The integrated signal difference $M(t)=|E_T'|^2-|A_bE_R|^2$ vs time for the receiver laser: (a) external modulation of peak intensity, (b) pump modulation by 50%. The broken line is the discrete bit values encoded on the transmitter laser. For the pump modulation scheme (b), the signal is encoded in the difference between the positive and negative maxima of the integrated signal difference across the intensity maxima. (c) Magnification of the region $525<t<535$ of part (b) showing the decoding of a ''-1'' bit (left) and ''1'' bit (right).

the transmitter laser. Although it is drawn as a continuous line, the value of the encoded bit only has meaning across the intensity peak. In these figures we plot $M(t)\equiv|E_T'|^2-|A_bE_R|^2$ vs t, where $|E_T'|^2$ is the intensity of the modulated transmitter laser at the receiver laser. Positive values of $M(t)$ can be associated with a transmitted ''1'' bit and negative values of $M(t)$ can be associated with a ''-1'' bit. Figure 7(b) shows a decoded message bit when the pump is modulated by $\pm50\%$ to encode the signal. The signal is again decoded by the integrated signal difference $M(t)$ and the dashed line in this figure is the value of the discrete bits ''±1'' encoded on the transmitter laser. The first two ''blips'' ($t<490$) in Fig. 7(b) represent no signal encoded. The encoding of signals consisting of random values of ''±1'' beginning at $t>490$. Note that $M(t)$ in Fig. 7(b) is neither all positive nor all negative as is essentially the case when the signal is encoded by modulating $|E_T|^2$ outside the laser, such as in Fig. 7(a). Figure 7(c) shows a magnified view of the region $525<t<535$ of Fig. 7(b) where a ''-1'' (left pulse) and ''1'' bit were decoded from the signal. For the ''1'' bit the positive area is slightly larger than the negative area leading to an overall positive integrated area, while

the reverse is true for the ''−1'' bit. Again, positive values of $M(t)$ can be associated with a ''1'' bit encoded on the transmitter laser and negative values of $M(t)$ can be associated with a ''−1'' bit. Net magnitudes of $M(t)$ clustered around zero can be interpreted as no signal sent. For the case of encoding the signal by pump modulation, the receiver is synchronized to the modulated transmitter laser in all regions outside of the area of the receiver intensity peak. Under the peak the transmitter and receiver intensities are slightly out of synchronization, yet still mutually entrained, with the receiver lagging the transmitter, leading to the double humped decoded signals in Figs. 7(b) and 7(c).

We note that when this pump modulation scheme is used to encode the signal onto the transmitting laser, an intensity return map $I_T(n+1)$ vs $I_T(n)$, is again useless in deciphering the hidden signal, having an appearance similar to that of Fig. 2(a). In addition, we also explored signal encoding with pump modulations of 10% and 90%. For both these modulation values, the intensity vs ISI return maps are similar in structure to Fig. 6, i.e., the encoded bit surfaces nearly coincide with the no-signal surface and they are all intertwined. The signals again could be decoded by an integrated signal difference at the receiver. However, for weak modulations values (e.g., 10%) decoded bit values could occasionally be misinterpreted because the difference between the positive and negative areas in Fig. 7(b) was small enough that a signal could be interpreted as a nonsignal.

On the other hand, for stronger modulation values (e.g., 90%) the decoding would occasionally fail, and decoded bits would be interpreted incorrectly. These instances would occur when perturbations to the transmitter carrier were enough to make it sufficiently dissimilar to the receiver that entrainment was momentarily lost for that signal pulse. As dicussed in Sec. II, the first term of Eq. (2.3) $-\kappa A_b \gamma_c (E_R - E_T)$ is responsible for the synchronization of the transmitter laser to the receiver laser. If the second term $\kappa \gamma_c (A_S - A_b) E_T$ is small with respect to the first term, the transmitter carrier wave plus signal can still be entrained by the receiver laser. However, for large pulse modulations this second term may, on occasion, not be small, and across this spiky peak entrainment is lost. In general, it appeared that intermediate values of the modulation (around 50%) produced the best results for reliably decoding the message at the receiver.

In a final numerical experiment, we explored the consequences of quasiperiodically modulating the loss coefficient of both the transmitter and receiver laser. The form of the modulation was modified to

$$\alpha(t) \equiv \alpha_0 + \alpha_1 [\cos(\Omega t) + a_2 \cos(f_2 \Omega t) + a_3 \cos(f_3 \Omega t)], \tag{4.1}$$

where the amplitudes $\{a_2, a_3\}$ and frequencies multipliers $\{f_2, f_3\}$ are fixed, but arbitrarily chosen constants. Again the receiver was operated at conditions for optimal synchronization $\alpha_{0R} = \alpha_{0T} + \kappa A_b$, and noise (typical for these lasers) was included in the calculations.

When a single additional frequency was used, ($a_2 \neq 0, a_3 = 0$ and $f_2 \neq 0, f_3 = 0$), the branches of the two-dimensional intensity-ISI return maps [as in Fig. 5(b)] *thickened and merged* as the amplitude a_2 approached unity. This thickening and merging effect was pronounced when two

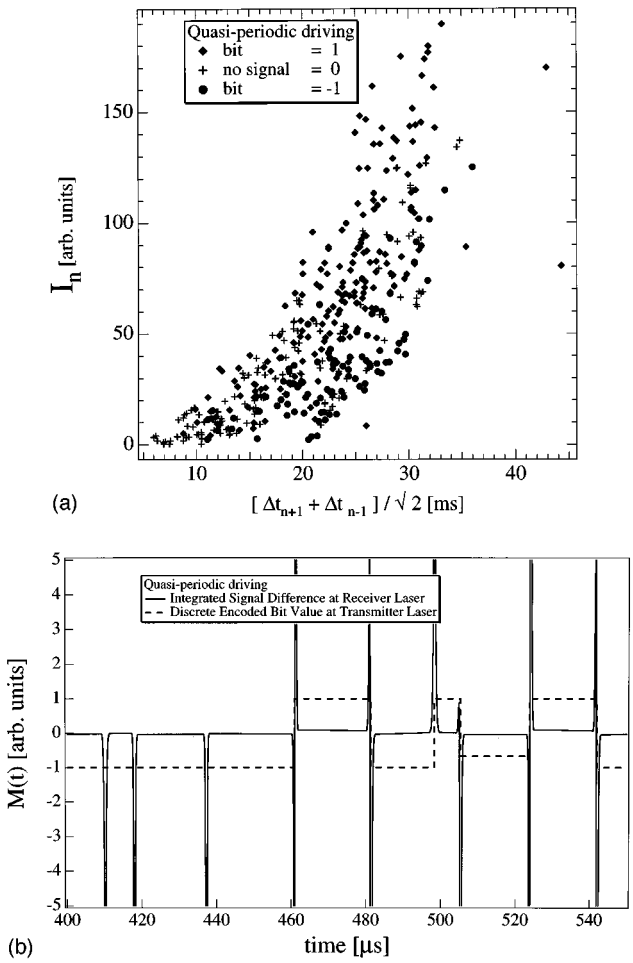

FIG. 8. Quasiperiodic driving of the loss coefficient of both the transmitter and receiver lasers: (a) intensity maxima vs ISI of the transmitter laser, (b) $M(t) = |E_T'|^2 - |A_b E_R|^2$ vs time for the receiver laser. The broken line is the discrete value of the decoded bit. By adding more driving frequencies (a), the signal branches of Fig. 5(b) are thickened and intermixed. However, the integrated signal difference at the receiver laser Fig. 8(b) can still decipher the hidden message.

additional frequencies were utilized. Figure 8(a) shows the intensity vs ISI return map for the transmitter laser for the case $a_2 = a_3 = 1$, with a choice of incommensurate relative frequencies $f_2 = \sqrt{2}$ and $f_3 = (\sqrt{5} - 1)/2$. Quasiperiodic driving led to an increase in the dimensionality of the attractor, exhibited by the thickening and merging of the intensity vs ISI map in Fig. 8(a). This renders the intensity vs ISI map ineffectual for deciphering the hidden message from the transmitter laser alone. The effect was qualitatively the same when additional commensurate frequencies were added to the driving. However, when utilizing commensurate frequencies, the remnants of the separate attractor surfaces for the encoded bits [as in Fig. 5(b)] could be inferred, if barely. However, the surfaces were thickened and merged enough, as in Fig. 8(a), to render the intensity vs ISI map ineffectual as a deciphering tool.

With no signal encoded, the transmitter synchronized effortlessly to the receiver laser. When the signal was encoded by amplitude modulation external to the transmitter laser (as in [6]), the signal could be decoded at the receiver laser by

means of an integrated signal difference, as evidenced in Fig. 8(b). Occasionally there were misinterpretations of the decoded bits for reasons similar to those discussed above for the case of encoding with pump modulations. We purposely increased the dimension of the attractor by adding more driving frequencies of arbitrary amplitude. Therefore, when a signal is impressed upon the transmitter carrier wave, it is occasionally different enough from the receiver signal so that the second term on the right-hand side of Eq. (4.1) perturbs the system enough so that entrainment is lost for this signal peak. The details of the modification of the local Lyapunov spectrum in the presence of multiple driving frequencies was not investigated, but would make for an interesting topic of exploration.

V. SUMMARY AND CONCLUSIONS

We have investigated the chaotic loss-modulated Nd:YAG laser and have found, both numerically and experimentally, that a return map utilizing intensity maxima and interspike intervals (ISI) reveals a regular, almost planar structure. This observation indicates that a simple relationship exists between the intensity maxima and the interspike intervals centered about that maxima, i.e., $I_T(n)=F[\Delta t_T(n+1),\Delta t_T(n)]$. In fact, by plotting the nth intensity maxima $I(n)$ versus the difference between the succeeding and preceding interspike intervals, i.e., $[\Delta t_T(n+1)-\Delta t_T(n)]/\sqrt{2} = [t(n+1)-t(n-1)]/\sqrt{2}$, we observe a nearly one-dimensional, one to one relationship between these variables, even in the presence of noise. This relationship was observed in numerical simulations as well as in experimental data taken at slightly different parameter values, leading to a variation of the interspike intervals on a much finer scale. However, even in this latter case, a plot of the intensity maxima-ISI return map reveals an almost planar structure and therefore a relationship between physical variables. Such a result would be useful, for example, in time series prediction of the future intensity maxima. In constructing the intensity-ISI return map it was not essential that the peak of the intensity be utilized. The ISI could have been defined relative to some arbitrary threshold value under the region of the peak and the return map then reconstructed.

The relationship between the the intensity maxima of the laser and the interspike intervals has consequences for the use of a transmitter-receiver pair of chaotic loss-modulated Nd:YAG lasers as a system to transmit encoded messages privately. By plotting the intensity-ISI return map of the transmitter laser alone, the message of ''$\pm$ 1'' bits, encoded by means of external cavity modulation, appears on surfaces above and below the no-signal surface. Even in the presence of moderate noise, the message can be deciphered.

As an alternative encoding scheme, we suggest encoding the signal by modulating the pump across the intensity maxima. This intrinsically perturbs the ISI of the transmitter laser, as opposed to the above externally modulated encoding scheme. The subsequent attempt to decode the embedded message by means of intensity-ISI return maps of the transmitter laser alone is unsuccessful because the *signal* attractor surfaces are merged onto the no-signal attractor surface. However, the message can still be decoded by means of driving the receiver laser with the output of the transmitter laser and extracting the message from an integrated intensity difference.

In addition, quasiperiodic driving of the loss coefficient of both the transmitter and receiver laser produced an increase in the dimensionality of the system. This led to a thickening of the intensity-ISI return maps with the merging of the individual surfaces corresponding to the $\{1,0,-1\}$ encoded bits. This rendered the intensity-ISI return maps ineffectual as means to decipher the signal from the transmitter laser alone. However, the signal could once again be extracted by means of an integrated signal difference at a receiver laser synchronized to the transmitter carrier wave.

Finally, the lessons learned in this study are twofold. First, an intensity-ISI or purely ISI return map can be a useful tool in the study of a pair of loss-modulated Nd:YAG lasers because of the implicit relationship between the intensity peak to the interspike intervals centered about that peak. Second, as applied to chaotic communications, the intensity-ISI return maps can be used to decipher the hidden message from the transmitter carrier wave alone. Care must be taken to intrinsically perturb the system or to increase the dimensionality of the system (though not high enough to void synchronization) so that the signal is safe from undesired deciphering by means of mapping techniques.

ACKNOWLEDGMENTS

The authors would like to thank the Maui High Performance Computer Center and the Albuquerque Research Center for the use of their parallel computing facilities during this work. R.R. would like to acknowledge support from the Division of Chemical Sciences, Office of Basic Energy Sciences, Office of Energy Research, U.S. Department of Energy, and the Office of Naval Research.

[1] L. M. Pecora and T. L. Carroll, Phys. Rev. A **44**, 2374 (1991); W. L. Ditto and L. M. Pecora, Sci. Am. (Int. Ed.) **269**, 62 (1993); N. Gershenfeld and G. Grinstein, Phys. Rev. Lett. **74**, 5024 (1995); E. Ott and M. Spano, Phys. Today **48**, 34 (1995); L. Kocarez and U. Parlitz, Phys. Rev. Lett. **74**, 5028 (1995); T. C. Newell, P. M. Alsing, A. Gavrielides, and V. Kovanis, Phys. Rev. E **51**, 2963 (1995).

[2] K. M. Cuomo and A. V. Oppenheim, Phys. Rev. Lett. **71**, 65 (1993).

[3] S. Hayes, C. Grebogi, E. Ott, and A. Mark, Phys. Rev. Lett. **73**, 1781 (1994); S. Hayes, C. Grebogi, and E. Ott, *ibid.* **70**, 3031 (1993).

[4] R. Roy and K. S. Thornburg Jr., Phys. Rev. Lett. **72**, 2009 (1994).

[5] T. Sugawara *et al.*, Phys. Rev. Lett. **72**, 3502 (1994).

[6] P. Colet and R. Roy, Opt. Lett. **19**, 2056 (1994).

[7] C. R. Mirasso *et al.*, IEEE Photonics Technol. Lett. **8**, 299 (1996).

[8] G. Pérez, and H. Cerdeira, Phys. Rev. Lett. **74**, 1970 (1995).
[9] L. Fabiny, P. Colet, R. Roy, and D. Lenstra, Phys. Rev. A **47**, 4287 (1993).
[10] T. Sauer, Phys. Rev. Lett. **72**, 3811 (1994).
[11] F. Taken, in *Dynamical Systems and Turbulence*, edited by D. A. Rand and L. L. Young, Lecture Notes in Mathematics Vol. 898 (Springer-Verlag, Berlin, 1981).
[12] I. B. Schwartz and T. Erneux, SIAM (Soc. Ind. Appl. Math.) J. Appl. Math. **54**, 1083 (1994).